Impact of winter blocking on surface air temperature in East Asia: Ural versus Okhotsk blocking

Jaeyoung Hwang[1], Seok-Woo Son[1]

Patrick Martineau[2,3], and David Barriopedro[4]

1. School of Earth and Environmental Sciences, Seoul National University, Seoul, Republic of Korea.
2. Japan Agency for Marine-Earth Science and Technology, Yokohama, Japan
3. Research Center for Advanced Science and Technology, University of Tokyo, Tokyo, Japan
4. Instituto de Geociencias, Consejo Superior de Investigaciones Científicas - Universidad Complutense de Madrid (CSIC-UCM), Madrid, Spain

Corresponding Author: Seok-Woo Son, School of Earth and Environmental Sciences, Seoul National University, 1 Gwanak-ro, Gwanak-gu, Seoul 08826, Republic of Korea.

E-mail: seokwooson@snu.ac.kr. Phone: +82-2-880-8152.

Abstract

Atmospheric blockings and their impacts on wintertime surface air temperature in East Asia are investigated by using three blocking indices. Blockings in two specific regions that indirectly or directly modulate East Asian climate variability are analyzed: Ural (UR) blocking over East Asia's northwest and Okhotsk (OK) blocking over East Asia's northeast. Both lead to cold anomalies in East Asia but through slightly different mechanisms. In the typical case of UR blocking, cold air associated with a mid-level trough develops to the east of the quasi-stationary blocking and slowly moves southeastward as the Siberian high intensifies. Four days after the blocking onset, East Asia experiences significant cooling due to the temperature advection associated with anomalous temperature gradient and adiabatic cooling. During the typical OK blocking event, a preexisting cold anomaly over northern Eurasia is pushed southeastward by the westward expansion of the blocking. The anomalous meridional flow due to blocking-induced dipolar circulation over the North Pacific further reinforces the cold advection over East Asia, with a minor contribution of vertical processes. In both types of blocking, the cold anomaly persists even in the decaying phase, due to an offset between the temperature advection and the diabatic heating.

Keywords: Ural blocking, Okhotsk blocking, Surface air temperature, East Asia

1. Introduction

A quasi-stationary high-pressure system, commonly referred to as atmospheric blocking, is one of the major features of mid-latitude weather systems. The associated circulation anomalies affect surface weather in a major way not only in the vicinity of the blocked region (e.g. Pfahl and Wernli 2012) but also over a considerably large area surrounding the blocking high (e.g. Wang et al. 2010; Sousa et al. 2018). Due to its persistence, blocking is particularly related to extreme events. For instance, many studies in the past two decades have documented that blocking is highly associated with cold surges (Park et al. 2011; Martineau et al. 2017), heat waves (Matsueda 2011), severe droughts (MacDonald 2007; García-Herrera et al. 2019), and heavy rainfall events (Hong et al. 2011; Lau and Kim 2012; Sousa et al. 2017). More recently, blocking has received attention as an important contributor to air stagnation and high concentrations of surface ozone and particulate matter (PM) (Garrido-Pérez et al. 2017; Ordóñez et al. 2017; Yun and Yoo 2019; Maddison et al. 2021), which pose a significant health risk.

Climatologically, blocking tends to occur near the upper-level jet exit and the storm track regions. In the Northern Hemisphere, blocking is most frequently found over the Euro-Atlantic and North Pacific basins. Although minor, blocking is also observed to the west of Russia or the Ural region (Lupo and Smith 1995; Barriopedro et al. 2006; Tyrlis and Hoskins, 2008). East Asia is far from these preferred blocking regions. However, it is well documented that East Asian surface weather is substantially influenced by high-latitude blocking especially in boreal winter, when blocking is most prominent (Tibaldi et al. 1994; Wiedenmann et al. 2002; Hwang et al. 2020). Previous studies reported that cold surges in East Asia are often caused by Ural (UR) blockings, which favor the development of quasi-stationary Rossby wave trains (Joung et al. 1982; Takaya and Nakamura 2005a; Park et al. 2014; Shi et al. 2020). Since East Asian surface weather is influenced by major teleconnection patterns, such as the Arctic Oscillation (e.g., Yoo et al. 2019), several studies have investigated the combined effect of UR blocking and atmospheric teleconnections (e.g., Shi et al. 2020). The Okhotsk (OK)

blocking, also referred to as Kamchatka or western North Pacific blocking, can also affect East Asian surface weather. Takaya and Nakamura (2005b) and Park et al. (2014) documented that the cold advection induced by OK blocking can bring wintertime cold surges in the region. Song et al. (2016) and Song and Wu (2021) further reported that cold anomalies in East Asia are associated with an enhanced East Asian trough accompanying OK blocking.

The above-mentioned studies have robustly documented that surface air temperature (SAT) over East Asia tends to decrease in response to both UR and OK blockings through horizontal temperature advection. However, the exact mechanism, including the relative importance of zonal versus meridional temperature advection and the contribution of adiabatic versus diabatic heating, is not fully understood, particularly during OK blockings. The role of the background flow compared to the anomalous circulation is also not well documented. Most importantly, the differences between UR and OK blocking impacts on East Asian surface weather are not explored in terms of the blocking-induced SAT anomaly structure, amplitude, and evolution.

The study of dynamics and impacts of blocking is challenging because there are too many definitions of blocking, which can include different types of high pressure systems (e.g., Sousa et al. 2021). The blocking detection algorithms and indices that are widely used in the literature can be conceptually grouped into three categories: i.e., anomaly-based index, gradient-reversal index, and their combination (or mixed index) (Woollings et al., 2018). Each index emphasizes different aspects of blocking (e.g., Barriopedro et al. 2010). For instance, the anomaly-based index (e.g., Dole and Gordon 1983) detects blocking as a quasi-stationary geopotential height anomaly of large amplitude but often includes quasi-stationary ridges. In the gradient-reversal index (e.g., Tibaldi and Molteni 1990), blocking is identified from the reversal of the meridional gradient of geopotential height. It occasionally misses immature or omega-type blocking. The mixed index partly resolves limitations of these two indices by combining them (Barriopedro et al. 2010; Dunn-Sigouin et al. 2013), but still suffers from arbitrary thresholds (Chan et al. 2019). Since blocking statistics and impacts are sensitive

to the choice of the blocking index (Doblas-Reyes et al. 2002; Barnes et al. 2014; Kim and Kim 2019), it was proposed to consider multiple indices to assess the robustness of the results (Woollings et al. 2018). A multi-index evaluation, utilizing the anomaly-based index, gradient-reversal index, and mixed index, is particularly useful for a comprehensive description of complementary blocking aspects.

The goal of the present study is to better understand and quantify the blocking impacts on East Asian SAT in boreal winter. Unlike previous studies which have considered either UR or OK blocking, both blocking types are considered. The uncertainty in the blocking statistics is reduced by examining the three different blocking indices. Most importantly, the mechanism through which UR and OK blockings affect East Asian SAT anomalies is investigated by analyzing the temperature tendency equation near the surface.

The paper is organized as follows. In Section 2, data, blocking indices, and the temperature tendency equation are described. Section 3a shows the 40-yr climatology of blocking frequency in the Northern Hemisphere, focusing on UR and OK blockings during the extended winter season. Their impacts on East Asian SAT anomaly and the mechanisms are investigated in Sections 3b and 3c. The conclusions are provided in Section 4.

2. Data and Method

a. Data

Data from the Japanese 55-year Reanalysis (JRA-55; Kobayashi et al. 2015) is used for the extended winter (November to March), from January 1979 to December 2018. Daily geopotential height at 500-hPa (Z500) is employed for detecting blockings. Daily SAT, mean sea level pressure (MSLP), and horizontal wind at 850 hPa are used to evaluate blocking impacts. The temperature tendency equation is computed from 6-hourly 925-hPa horizontal wind (u, v), temperature (T925),

pressure velocity (ω), and diabatic heating rates. The model-predicted parameterized diabatic heating rates are derived from the convective heating (cnvhr), large-scale condensation (lrghr), short-wave radiation (swhr), long-wave radiation (lwhr), and vertical diffusion (vdfhr). Variables are analyzed at a 2.5º longitude by 2.5º latitude resolution.

b. Blocking indices

Following Woollings et al (2018), three blocking indices are adopted to identify UR and OK blocking events. They are the anomaly-based (ANO) and gradient-reversal (REV) indices, which are based on the two standard approaches (i.e., Dole and Gordon 1983; Tibaldi and Molteni 1990), as well as the mixed (MIX) index. The details of these algorithms are described below. The ANO index solely considers Z500 anomaly (Woollings et al. 2018). First, the daily Z500 anomaly, which is defined as a deviation from the daily climatology (i.e, daily-mean seasonal cycle), is computed. The amplitude threshold is calculated as the standard deviation of daily Z500 anomalies for each calendar month by using all grid points within 30º to 80ºN over a three-month window. For instance, the threshold for April's days is derived from daily Z500 anomalies from March to May. If the local Z500 anomaly is greater than 1.3 standard deviation, it is assigned as a blocking candidate. Only the blocking candidates that occupy an area larger than 2.0×10^6 km^2 and overlap more than 50% within consecutive days for at least 5 days are classified as blocking. The present study seeks to identify blocking events occurring within 30º to 80ºN to avoid the detection of subarctic systems.

An example of OK blocking detected by the ANO index is illustrated in Fig. 1a. An enhanced anticyclonic Z500 anomaly is observed over the Okhotsk region. The blocked area covers the entire Okhotsk region and is centered on the maximum positive Z500 anomaly. Since the index groups contiguous grid points with the anomaly greater than the threshold, the positive anomaly in the latitude below 45ºN (180º-160ºW) is also considered as being part of the blocking.

The REV index detects the area satisfying the reversal of meridional gradient of Z500 as in Scherrer et al. (2006) and Davini et al. (2012). The Z500 gradient is computed as below:

$$GHGN(\lambda,\phi) = \frac{Z500(\lambda,\phi+\Delta) - Z500(\lambda,\phi)}{\Delta} < -10\ m/^\circ$$

$$GHGS(\lambda,\phi) = \frac{Z500(\lambda,\phi) - Z500(\lambda,\phi-\Delta)}{\Delta} > 0\ m/^\circ \quad (1)$$

$$GHGS2(\lambda,\phi) = \frac{Z500(\lambda,\phi-\Delta) - Z500(\lambda,\phi-2\Delta)}{\Delta} < -5\ m/^\circ$$

where, λ and ϕ are longitude and latitude, respectively, and Δ is set to 15°. $GHGN(\lambda,\phi)$, $GHGS(\lambda,\phi)$, and $GHGS2(\lambda,\phi)$ are evaluated for ϕ within 45°-70°N at each longitude λ and averaged zonally over the $\Delta/2$ longitudinal sector to smooth out small scale perturbations. When the resulting quantities satisfy the above criteria in Eq. (1), the grid point is considered as a blocking candidate. As in Woollings et al. (2018), the minimum blocking area is set to 5.0×10^5 km^2. When the detected blocking area satisfies the overlapping conditions as in the ANO index, it is classified as a blocking.

The OK blocking example of Fig. 1 detected by the REV index is shown in Fig. 1b. As compared to the ANO index (Fig. 1a), the REV blocking is detected over a region with relatively weaker Z500 anomalies (50°-70°N, 120°-140°E) because the REV index detects only the reversal of Z500 gradient. This result clearly shows that the blocked regions detected by different blocking indices can differ to a large extent.

The MIX index, which was first introduced by Barriopedro et al. (2010), is based on both ANO and REV indices. It seeks Z500 anomaly with the same criteria used in the ANO index, but additionally imposes the flow reversal criteria of Eq. (2), following Dunn-Sigouin et al. (2013)[1]:

[1] Note that the sign of $Gr(i^*)$ in Eq. (3) of Dunn-Sigouin et al. (2013) should be positive.

$$GHGN(\lambda,\phi) = \max[Z500(\lambda,\phi) - Z500(\lambda,\phi-\Delta\phi)] \ > \ 0 \quad (2)$$

$$\lambda_{max} - \Delta\lambda/2 \ < \ \lambda \ < \ \lambda_{max} + \Delta\lambda/2$$

$$\phi_{max} - \Delta\phi/2 \ < \ \phi \ < \ \phi_{max} + \Delta\phi/2$$

where, λ_{max} and ϕ_{max} are longitudinal and latitudinal locations of the maximum Z500 anomaly, $\Delta\lambda$ and $\Delta\phi$ is set to 10° and 15°, respectively. This index looks for an amplified Z500 anomaly accompanying a meridional Z500 gradient reversal. It implies that the blocked region diagnosed by the MIX index should be identical to the region identified by the ANO index, as long as the blocking event is detected by both indices. Since the OK blocking shown in Fig. 1 is detected by both the ANO and MIX, the blocked region detected by the MIX index is the same as Fig. 1a.

To assess the blocking impacts on East Asia SAT, we first select the blocking events whose maximum Z500 anomalies are located within the sector spanning 30°-180°E and 50°-80°N and persist therein during at least 5 days. The onset day is defined as the first day when the blocking is detected in this sector. If the maximum anomaly is located within 30°-100°E (red box in Figure 2) at the onset day, it is classified as a UR blocking. A similar approach was taken by Cheung et al. (2013), Yao et al. (2017), and Chen et al. (2018). In this way, a total of 118, 90, and 109 events are identified by the ANO, MIX, and REV indices over the Ural region, respectively (Table 1). Likewise, OK blocking is identified when the maximum blocking anomaly is first detected within 100°-180°E (green box in Fig. 2). A total of 86, 66, and 89 events are identified over the Okhotsk region for the three indices (Table 1). It is noted that the zonal band for identifying OK blocking covers the far east region from the Okhotsk sea, since the maximum blocking-like low-frequency variability is often located over Bering seas (Kushnir 1987). Although not shown, the overall results do not change much when the detection domain is slightly changed to 100°-160°E or 120°-180°E. It is also noteworthy that blockings occasionally occur simultaneously over both sectors. However, the number of such cases is relatively small, and they are not treated separately.

c. Thermodynamic equation

The blocking impact on SAT over East Asia (105°-145°E, 20°-50°N; see the black box in Fig. 1) is examined by calculating the thermodynamic equation at 925 hPa:

$$\left(\frac{\partial T}{\partial t}\right)' = -(\boldsymbol{V}\cdot\nabla T)' + \left(\omega S_p\right)' + Q' + \mathrm{RES} \quad (3)$$

where $\partial \mathrm{T}/\partial t$ is the temperature tendency at 925 hPa (OBS); $-\boldsymbol{V}\cdot\nabla T$ is the horizontal advection (ADV); ωS_p is the adiabatic heating (VER). Q is total diabatic heating (DIA), which is obtained by adding the diabatic heating rates from cnvhr, lrghr, lwhr, swhr, and vdfhr. Residual (RES) is defined as the difference between the observed tendency and budget tendency. Primes denote anomalies calculated as departures from the daily climatology (i.e., raw data minus its daily-mean seasonal cycle). $\boldsymbol{V}$ and ω are the horizontal wind vector and pressure velocity ($\mathrm{Pa\,s^{-1}}$), respectively. S_p $\left(= RT/pC_p - \partial T/\partial p\right)$ stands for the stability parameter, with R (287 $\mathrm{J\,kg^{-1}\,K^{-1}}$) and C_p ($1004\,\mathrm{J\,kg^{-1}\,K^{-1}}$) being the specific gas constant for dry air and the specific heat capacity. ∇ is the horizontal gradient operator. The choice of the pressure level is justified by its proximity to surface. Furthermore, it allows the computation of adiabatic heating, for which it is necessary to evaluate vertical gradients.

3. Results

3.1. Climatology of Ural and Okhotsk blockings

The climatology of Northern Hemisphere blocking frequency in November-March is depicted in Fig. 2 for three blocking indices. The spatial distribution is qualitatively similar across all three blocking indices; blocking is frequently observed over the North Pacific and the Euro-Atlantic sectors.

196 However, non-negligible differences between indices are also evident, in agreement with previous
197 studies (e.g., Woollings et al. 2018).

198 In the case of the ANO index, two local maxima in blocking frequency appear over the North
199 Atlantic and North Pacific oceans with the largest spatial extent among the three indices (Fig. 2a).
200 Another preferred region of blocking frequency is located over the Ural region, which can be viewed
201 as an extension of Euro-Atlantic blocking. The blocking frequency detected by the MIX index is
202 similar to that of the ANO index except for the overall reduced frequency (Fig. 2b). As can be inferred
203 in Table 1, the MIX index detects fewer blocking events than the ANO index. This is anticipated
204 because the MIX index excludes quasi-stationary ridges which are occasionally detected as blocking
205 events in the ANO index (Barriopedro et al. 2010). The difference between ANO and MIX is much
206 larger over the North Pacific sector because quasi-stationary ridges, which are frequently observed
207 over that region (Hansen and Sutera 1993; Miller et al. 2020; Sousa et al. 2021), are effectively reduced
208 by the MIX index (Dunn-Sigouin et al. 2013).

209 The frequency of blocking derived from the REV index shows a meridionally confined spatial
210 distribution (Fig. 2c). This is partly explained by the fact that the flow reversal regions, depicted by
211 the REV index, are usually smaller than the blocking anomaly captured by the ANO and MIX indices.
212 The centers of blocking activities are also slightly different than in the ANO and MIX indices.
213 Compared to the other indices, the region of maximum blocking frequency is shifted eastward in the
214 Euro-Atlantic sector but westward in the North Pacific sector. As a consequence, regional blocking
215 activity over Greenland (Hanna et al. 2016) is well distinguished from the Euro-Atlantic blocking by
216 the REV index.

217 It is also noteworthy that the blocking frequency over the North Pacific becomes much larger
218 than over the Euro-Atlantic sector when the poleward criterion is lessened (i.e., $GHGN(\lambda, \phi) = 0$). It
219 indicates that North Pacific blocking is more sensitive to the poleward criterion (compare Fig. 2c and

Fig. S1 of the Supporting Material), suggesting that not only the choice of blocking index (e.g., Kim and Kim 2019) but also the criterion of the index (e.g., Tyrlis et al. 2021) need to be considered. However, our results are overall not very sensitive to the poleward criterion, except for the number of identified blocking events (not shown).

Figure 2 confirms that Northern Hemisphere blockings are most frequent at the exit region of the upper-level jet, especially on its poleward side (e.g., Nakamura and Huang 2018). It is also clear that blocking is relatively rare over East Asia. However, as shown below, East Asian surface weather is substantially affected by high-latitude blockings over Ural and Okhotsk regions. Figure 3 shows the spatial distribution of regional blockings over the Ural and Okhotsk regions. For all indices, the maximum frequency of UR blocking is found at 60ºE and 60ºN (Figs. 3a-c), in agreement with Cheung et al. (2013). Likewise, the maximum frequency of OK blocking is consistently detected at 160ºE and 60ºN (Figs. 3d-f). Note that UR and OK blockings display a zonally elongated distribution from the maximum frequency region, which may reflect the eastward or westward progression of blocking.

The time series of normalized UR and OK blocking frequencies identified by the three indices are depicted in Fig. 4. Not surprisingly, interannual variability is considerably similar between the ANO and MIX indices. Their correlation is the largest ($r > 0.7$) of all blocking indices for both UR and OK blockings. These indices also show a high correlation ($r \sim 0.6$) with the REV index for the UR blocking region. However, the OK blocking frequency detected by the REV index exhibits relatively lower correlations with the corresponding ANO and MIX series ($r = 0.46$ and 0.59, respectively). Although all values are still statistically significant at the 99% confidence level, this result indicates that there is an uncertainty in detecting UR and OK blocking and that the multi-index approach is useful to reduce it. In the next section, the impacts of these regional blockings on East Asian SAT are quantified.

3.2. Impacts of Ural and Okhotsk blockings

The daily composite maps are constructed with respect to the life cycle of blocking for each index. They are then averaged across all three indices to collectively quantify the blocking impacts. The results are considered robust when all three indices show same signed anomalies and statistically significant differences ($p < 0.05$) from the climatology (dashed). For reference, some results are also separately reported for each index in the supporting materials (Figs. S2 and S3).

Figure 5 illustrates the spatio-temporal evolution of UR blocking and associated MSLP and SAT anomalies from lag -4 to 9 days with respect to blocking onset. The Z500 (Figs. 5a,d) and MSLP anomalies (Figs. 5b,e) start to amplify several days before the blocking onset and exhibit progressive intensification. Although not significant, cold anomalies already appear over Eurasia in this early stage (Figs. 5c,f).

At the onset day, UR blocking is co-located with the amplified ridge, with a quasi-barotropic anomalous circulation (Figs. 5g,h). An anomalous cyclonic circulation also appears downstream (90ºE and 40ºN), indicating the westward deepening or broadening of the Asian trough over time. As the anticyclonic anomaly develops (middle panels in Fig. 5), Eurasian SAT gets colder, and the Arctic SAT over the Barents-Kara seas (north of the Ural region) becomes warmer. The resulting SAT pattern (Fig. 5i) is often referred to as the Warm Arctic Cold Eurasia (WACE) pattern (e.g., Mori et al. 2014; Kim and Son 2016; Luo et al. 2016; Tyrlis et al. 2020; Kim and Son 2020; Kim et al. 2021).

As the blocking further develops, Z500 and MSLP anomalies at lag 2 to 4 days remain quasi-stationary over the Ural region, leading to a well-organized anticyclonic circulation at 925 hPa (vectors in Figs. 5k,n). Consequently, the WACE pattern expands and becomes more pronounced (Figs. 5l,o). The positive MSLP anomaly slowly expands southward on its eastern edge from lag 2 to 6 days (Figs. 5k,n,g). Although weak, a negative MSLP anomaly moves eastward around this time, likely associated

with an eastward migration of cyclonic anomaly downstream of UR blocking (Figs. 5j,m,p). It allows southward expansion of the MSLP anomaly from central Eurasia (Yihui 1990; Shi et al. 2020).

At lag 4 days, the cold anomaly reaches East Asia on the east of the Tibetan Plateau, showing statistically significant cooling over the region. After that, the southeastward propagation of cold air slows down (Figs. 5r), showing a horseshoe shape due to the barrier effect of the Tibetan Plateau (see also Fig. 8a). Despite the decay of UR blocking (Fig. 5s), the cold anomaly remains with the established positive MSLP anomaly over East Asia at lag 9 days (Figs. 5t,u).

The same analysis is conducted for OK blocking (Fig. 6). Before the onset, an incipient Z500 anomaly is located at the jet exit region over the North Pacific (Fig. 6a), and a warm anomaly instead of a cold anomaly appears over East Asia (Fig. 6c). As blocking forms (Figs. 6d,g), the anticyclonic MSLP anomaly starts to expand westward (Takaya and Nakamura 2005b). This westward-elongation or expansion of OK blocking slightly differs from the quasi-stationary nature of UR blocking (compare left and middle columns of Figs. 5 and 6). With the blocking build-up, the East Asian trough deepens and the associated negative SAT anomaly over northern Eurasia (70°-130°E, 50°-80°N) is pushed southeastward (Figs. 6d-f), although this is not significant in the ANO index (Figs. S3a,d,g).

At the onset day, the blocking high is located over the Okhotsk region with anomalous cyclonic circulation over the southern North Pacific (130°-180°E, 20°-40°N), showing a cyclonic wave breaking (Masato et al. 2012) (Fig. 6g). The meridional dipole in Z500 anomaly becomes pronounced until lag 4 days. A similar dipole pattern is also observed in MSLP anomalies (Fig. 6h), implying that the barotropic structure is likely associated with the North Pacific Oscillation (e.g., Barriopedro et al. 2006; Sung et al. 2021). The East Asian surface temperature starts to further cool (Fig. 6i), due to northerly flows from the cyclonic circulation and the corresponding negative MSLP anomaly over the North Pacific. At lag 4 days, the positive MSLP anomaly expands southward on its western edge due to blocking-induced cyclonic circulation over the North Pacific (Figs. 6n,q). At the same time, the cold

anomaly becomes significant over East Asia (Figs. 6o,r). The positive MSLP reaches East Asia (Fig. 6t), and the cold anomaly remains over the region even at lag 9 days (Fig. 6u) despite the decay of OK blocking (Fig. 6s).

The comparison of Figs. 5 and 6 reveals that the SAT anomaly resulting from OK blocking is substantially weaker than that of UR blocking, partly due to the preexistence of warm SAT anomaly over the region (Fig. 6c). Moreover, the cold anomaly over East Asia during OK blocking covers the continent and ocean basins (Fig. 6r), whereas the SAT anomaly resulting from UR blocking is confined to the continent (Fig. 5r). However, if the net East Asian SAT change from lag -4 to 9 days is considered, SAT change associated with OK blocking is comparable to or slightly larger than that of UR blocking (as shown below).

Similar results are found when each blocking index is separately considered (Figs. S2 and S3), although common cases across the three indices account for only 50% of the regional blockings detected by the ANO and REV indices (Table 1). The differences across indices are somewhat more acute for OK than for UR blockings. For example, as compared to the other blocking indices, the MIX index shows a more pronounced surface cooling over East Asia during OK blocking development, which is presumably due to the preexisting cold anomaly over northern Eurasia (Figs. S3e,h,k).

Figure 7 quantifies the response time of SAT anomaly to UR and OK blockings averaged across the three blocking indices. The response time is somewhat sensitive to the choice of the blocking index (Fig. S4) and hence it is here defined as the first day when the negative SAT anomaly becomes statistically significant in three blocking indices at each grid point. The cold anomaly appears almost simultaneously with the onset of UR blocking (Fig. 7a). The accumulated cold anomaly then starts to expand towards the east and the west. While cooling advances southeastward along the eastern boundary of the Tibetan Plateau, it is also pushed southwestward by the anticyclonic blocking circulation, exhibiting a zonally elongated pattern from the Middle East to East Asia (Fig. 5r).

315 Differently, the SAT response to OK blocking is first detected over the North Pacific, and it expands
316 westward in the next few days (Fig. 7b).

317 To further understand the surface responses to blocking, Figure 8 depicts correlation maps
318 between East Asia SAT tendency and MSLP anomaly during the period of cooling tendency (i.e., lags
319 1 to 5 days for UR blocking and -1 to 3 days for OK blocking). The impact of UR and OK blockings
320 on cold East Asian anomalies is highly associated with an amplification of the climatological MSLP
321 over Siberia, in agreement with Takaya and Nakamura (2005a,b). Moreover, a significant positive
322 correlation is found over southern East Asia for both types of blocking, likely reflecting the effect of
323 the southward propagating cyclonic anomaly (see Figs. 5h,k,n and 6e,h,k). A more detailed
324 investigation of the physical processes associated with the East Asian cooling is addressed in the next
325 section.

326

327 **3.3. Mechanism of Blocking impacts.**

328 To understand the processes that drive the cold anomaly over East Asia, the SAT anomaly has
329 been averaged over the East Asian region, with each grid point weighted by the area it represents. The
330 resulting evolution of East Asian SAT anomaly is similar to that observed at 925 hPa for both UR (Fig.
331 9a) and OK (Fig. 10a) blocking. Accordingly, the contributing factors are hereafter assessed at the 925-
332 hPa level, as described in Section 2c (Eq. 3).

333 Although not statistically significant, temperature begins to decrease before the onset of UR
334 blocking, in agreement with Fig. 5. The cooling anomaly becomes statistically significant at lag 4 day
335 and persists for a few days (Fig. 9a). Figure 9b illustrates the observed T925 tendency (OBS), and the
336 three contributing terms of Eq. (3) as a function of time. A significant negative tendency appears from
337 lag 1 to 5 days (indicated by the white box). It turns out that cooling is mainly caused by horizontal
338 advection (ADV) and adiabatic cooling (VER), with a partial cancellation by total diabatic heating

(DIA). While both zonal (ADVx) and meridional (ADVy) advections contribute to East Asian cooling, meridional advection becomes dominant after lag 4 days, in agreement with Shi et al. (2020). Its cooling effect, however, is largely canceled out by diabatic heating, explaining the absence of additional cooling after lag 5 days.

The relative contribution of each term is summarized in Fig. 9c for the cooling period from lag 1 to 5 days. The budget tendency captures well the observed tendency over East Asia, with a small residual (orange bar). The ADV explains the majority of the negative tendency, and it is statistically significant in two out of three blocking indices. Although ADVy is not significant, its contribution is comparable to that of zonal advection. This result is consistent with the southeastward displacement of the cold anomaly downstream of UR blocking as shown in Figs. 5i,l,o. The contribution of VER to cooling tendency is of secondary importance, but it is robust across the blocking indices.

To elucidate the nature of ADV and VER terms, they are further decomposed into climatological and anomaly components, as follows:

$$-(\boldsymbol{V}\cdot\nabla T)' = (-\boldsymbol{V}'\cdot\nabla\bar{T}) + (-\bar{\boldsymbol{V}}\cdot\nabla T') + (-\boldsymbol{V}'\cdot\nabla T')' \quad (4)$$

$$\left(\omega S_p\right)' = \left(\omega'\overline{S_p}\right) + \left(\bar{\omega}S_p'\right) + \left(\omega' S_p'\right)' \quad (5)$$

where overbar denotes daily climatology, and prime indicates anomaly, which is a deviation from the daily climatology. The decomposed terms of ADV, i.e., $(-\boldsymbol{V}'\cdot\nabla\bar{T})$, $(-\bar{\boldsymbol{V}}\cdot\nabla T')$, and $(-\boldsymbol{V}'\cdot\nabla T')'$ are referred to as ADVac, ADVca, and ADVaa, respectively. Likewise, $\left(\omega'\overline{S_p}\right)$, $\left(\bar{\omega}S_p'\right)$, and $\left(\omega' S_p'\right)'$ in Eq. (5) are referred to as VERac, VERca, and VERaa, respectively. It is found that ADV is largely explained by ADVca and ADVaa (Figs. 9d,e) during the cooling period of UR blocking, indicating that the anomalous temperature gradient induced by the blocking circulation plays a major role in ADV. Although the contribution of ADVac is negligible in the cooling period, it acquires an important role thereafter by maintaining the cold anomaly (Fig. 9d) through the anomalous anticyclonic circulation over East Asia (Figs. 5q,t). The ADVca also acts against diabatic heating over

East Asia after the cooling period (Figs. 9b,d), indicating that the anomalous temperature gradient set by the amplified cold Siberian high plays a key role in sustaining the cold anomaly (Figs. 5r and 5q).

The VERac, which presumably measures the effect of anomalous vertical motions due to the eastward propagating cyclonic anomaly downstream of the blocking (Figs. 5j,m), explains most of the VER cooling. An eastward-propagating upward motion appears on the east of the Tibetan Plateau (Fig. S5). The upward motion is more pronounced at 500 hPa, indicating that it is associated with an organized synoptic weather system (e.g., Hsu 1987). These results stress that the local cyclonic circulation that accompanies UR blocking plays a non-negligible role in driving the East Asian cooling.

The DIA shows a significant warming effect, partly canceling out the negative tendency. This canceling effect is also significant across the indices. To elucidate the nature of diabatic warming, the decomposed components are depicted in Fig. 9f. The diabatic warming is mainly caused by longwave radiation over the continent, with a minor contribution of large-scale condensation over the ocean. The latter, likely associated with the local cyclonic anomaly, is in agreement with the adiabatic cooling, and shows robustness across the blocking indices (Fig. 9g). After the cooling period, diabatic heating gets stronger, canceling the cold advection (see lag 6 to 10 days in Fig. 9b). The increased diabatic heating is mainly due to sustained warming by longwave radiation and enhanced vertical diffusion from the warm ocean to the atmosphere.

Figure 10 shows the T925 budget analysis for OK blocking. In this case, the East Asian temperature anomaly also starts to decrease several days before the onset, but at a faster rate than for UR blocking. Accordingly, the East Asian cooling becomes significant just two days after the blocking onset (Fig. 10a), and persists several days.

The main period of cooling tendency (lag -1 to 3 days) is mostly explained by ADV, with a minor contribution of VER and a partial cancellation by DIA (Figs. 10b,c). Unlike UR blocking, the meridional advection (ADVy), mainly due to an anomalous cyclonic circulation over the North Pacific (Figs. 6h,k), clearly dominates ADV. Although the ADVy becomes more pronounced over time its

cooling effect is largely canceled by DIA after the cooling period. The contribution of each term for the cooling period is summarized in Fig. 10c. The ADV, through both of its subcomponents (i.e., ADVx and ADVy), explains the overall cooling tendency, showing statistically significant values in all three blocking indices. The VER also supports the East Asian cooling, but it is of secondary importance, whereas the diabatic warming partly cancels out the negative tendency in all blocking indices.

Although the T925 tendency is largely explained by ADV (especially ADVy) during both UR and OK blockings, the decomposition reveals its different nature. Unlike UR blocking, ADV is dominated by ADVac during OK blocking (compare Figs. 9e and 10e). Since ADVac represents the temperature advection by anomalous circulation in the presence of a spatial gradient in climatology, this result reveals the importance of circulation anomalies induced by OK blocking. Although weak, VERca also supports the cooling over East Asia, likely due to an increased static stability by cold surface conditions. Moreover, ADVaa, which represents the southward propagation of a preexisting negative temperature anomaly over northern Eurasia (Figs. 6c,f), also decreases East Asian temperature from lag -3 to -1 days. However, the contribution of ADVaa is of secondary importance and less robust across indices (see also Figs. S3d,e,f).

The contribution of diabatic heating during OK blocking is further decomposed in Fig. 10f. Different to UR blocking, the vertical diffusion accounts for the largest warming in DIA, with a secondary contribution of longwave radiation during the cooling period (see also Fig. 10g). In the maintenance period from lag 4 to 10 days, their contributions become stronger and more robust. Unlike UR blocking, the large-scale condensation tends to assist the East Asian cooling due to anomalous downward motion by upper-level convergence of the blocking-induced circulation (Figs. 6n,q).

4. Summary and Discussion

411 This study investigates the spatio-temporal evolution of Ural (UR) and Okhotsk (OK)
412 blocking events and their impacts on surface air temperature (SAT) over East Asia during the extended
413 winter season. The detailed mechanism(s) whereby these two types of regional blockings affect East
414 Asia is also investigated. The analysis presented here focuses on robust aspects to blocking definition
415 and discusses blocking-related uncertainties by performing a multi-index assessment as well as
416 sensitivity analyses with respect to the choice of blocking index.

417 When UR blocking forms, a cold SAT anomaly develops over the southeastern flank of the
418 blocking, while a warm anomaly appears over the northwest. The dipolar SAT anomalies resemble the
419 Warm Arctic-Cold Eurasia pattern. As the blocking reaches its maximum spatial extent and the
420 cyclonic anomaly downstream of UR blocking moves eastward, an amplified cold anomaly over
421 Siberia progresses southeastward along the eastern boundary of the Tibetan Plateau. Approximately
422 four days after the blocking onset, East Asia experiences significant cooling, which persists during the
423 blocking lifetime.

424 The OK blocking is preceded by a warm SAT anomaly over East Asia. Unlike the quasi-
425 stationary UR blocking, OK blocking tends to retrogress, displacing the preexisting cold anomaly over
426 northern Eurasia towards the southeast. The anticyclonic sea level pressure anomaly slowly moves
427 southwestward along the western boundary of a cyclonic anomaly over the western North Pacific. The
428 cold advection by the blocking-induced circulation drives a significant cooling over East Asia
429 approximately two days after the blocking onset, which persists for several days. As compared to UR
430 blocking, the East Asian SAT response to OK blockings is somewhat weaker, partly due to the
431 influence of a preexisting warm anomaly. However, when the cooling period is consideredthe SAT
432 change in response to OK blocking is comparable to that of UR blocking.

433 The processes responsible for blocking-induced SAT change are also elucidated through the
434 thermodynamic budget analysis of East Asian temperature change during the cooling period. In both

cases, horizontal temperature advection is most important with a minor contribution of adiabatic heating and partial cancellation by diabatic warming. However, their detailed mechanisms are slightly different. For UR blocking, both zonal and meridional cold advections associated with an anomalous temperature gradient set by the southward extended Siberian high account for a large fraction of East Asian cooling. The adiabatic cooling from anomalous vertical motion also plays a non-negligible role, and is associated with the development and subsequent eastward migration of a cyclonic circulation anomaly. This cyclonic anomaly may represent an enhanced lee cyclogenesis downstream of the Tibetan Plateau due to a deepening upper-level trough to the east of UR blocking as blocking develops. In the case of OK blocking, the temperature tendency over East Asia is mainly explained by the horizontal advection of cold air by the anomalous meridional flow with a minor contribution of the anomalous temperature gradient. This cold advection is mostly associated with the high-low dipolar configuration of the sea level pressure anomalies over the North Pacific.

The maintenance of the East Asian cooling has also been investigated. During UR blocking, the sustained cold advection by anticyclonic circulation over East Asia and southward expansion of the Siberian high is mostly canceled out by the diabatic warming from longwave radiation and vertical diffusion from the warm ocean to the cold atmosphere. Differently, the diabatic warming that prevents additional cooling by the OK blocking-induced cyclonic circulation mostly results from vertical diffusion over the warm ocean. Overall, all these results emphasize different mechanisms behind the otherwise similar impacts of UR and OK blocking on East Asian climate. These findings may contribute to improve our understanding of blocking-related impacts in climate models, including their biases (Brunner et al. 2018; Jury et al. 2019; Jeong et al. 2021) and changes in future climate (Masato et al. 2014).

Acknowledgement

Jaeyoung Hwang and Seok-Woo Son were supported by the R&D Program for Oceans and Polar Regions of the National Research Foundation (NRF) funded by the Ministry of Science and ICT(NRF-2020M1A5A1110579). Patrick Martineau was supported in part by the Japan Society for the Promotion of Science (JSPS) through Grant-in-Aid for Scientific Research JP19H05702 (on Innovative Areas 6102). David Barriopedro was supported by the Spanish Ministry of Science, Innovation and Universities through the JeDiS (RTI2018-096402-B-I00) project. The authors are grateful to two anonymous reviewers, who provided constructive comments and helped improve the manuscript.

References

Barnes, E. A., Dunn- Sigouin, E., Masato, G., & Woollings, T. (2014). Exploring recent trends in Northern Hemisphere blocking. *Geophysical Research Letters*, **41**(2), 638-644.

Barriopedro, D., García-Herrera, R., Lupo, A. R., & Hernández, E. (2006). A climatology of Northern Hemisphere blocking. *Journal of Climate*, **19**(6), 1042-1063.

Barriopedro, D., García-Herrera, R., & Trigo, R. M. (2010). Application of blocking diagnosis methods to general circulation models. Part I: A novel detection scheme. *Climate dynamics*, **35**(7-8), 1373-1391.

Brunner, L., Schaller, N., Anstey, J., Sillmann, J., & Steiner, A. K. (2018). Dependence of present and future European temperature extremes on the location of atmospheric blocking. *Geophysical research letters*, **45**(12), 6311-6320.

Chan, P. W., Hassanzadeh, P., & Kuang, Z. (2019). Evaluating indices of blocking anticyclones in terms of their linear relations with surface hot extremes. *Geophysical Research Letters*, **46**(9), 4904-4912.

Cheung, H. N., Zhou, W., Shao, Y., Chen, W., Mok, H. Y., & Wu, M. C. (2013). Observational climatology and characteristics of wintertime atmospheric blocking over Ural–Siberia. *Climate dynamics*, **41**(1), 63-79.

Chen, X., Luo, D., Feldstein, S. B., & Lee, S. (2018). Impact of winter Ural blocking on Arctic sea ice: short-time variability. *Journal of Climate*, **31**(6), 2267-2282.

Davini, P., Cagnazzo, C., Gualdi, S., & Navarra, A. (2012). Bidimensional diagnostics, variability, and trends of Northern Hemisphere blocking. *Journal of Climate*, **25**(19), 6496-6509.

Dee, D. P., Uppala, S. M., Simmons, A. J., Berrisford, P., Poli, P., Kobayashi, S., ... & Vitart, F. (2011). The ERA- Interim reanalysis: Configuration and performance of the data assimilation system. *Quarterly Journal of the royal meteorological society*, **137**(656), 553-597.

Doblas- Reyes, F. J., Casado, M. J., & Pastor, M. A. (2002). Sensitivity of the Northern Hemisphere

492 blocking frequency to the detection index. *Journal of Geophysical Research: Atmospheres*,
493 **107**(D2), ACL-6.
494 Dole, R. M., & Gordon, N. D. (1983). Persistent anomalies of the extratropical Northern Hemisphere
495 wintertime circulation: Geographical distribution and regional persistence characteristics.
496 *Monthly Weather Review*, **111**(8), 1567-1586.
497 Dunn-Sigouin, E., Son, S. W., & Lin, H. (2013). Evaluation of Northern Hemisphere blocking
498 climatology in the global environment multiscale model. *Monthly weather review*, **141**(2),
499 707-727.
500 Garrido-Perez, J. M., Ordóñez, C., & Garcia-Herrera, R. (2017). Strong signatures of high-latitude
501 blocks and subtropical ridges in winter PM10 over Europe. *Atmospheric Environment*, **167**,
502 49-60.
503 García-Herrera, R., Garrido-Perez, J. M., Barriopedro, D., Ordóñez, C., Vicente-Serrano, S. M.,
504 Nieto, R., ... & Yiou, P. (2019). The European 2016/17 drought. *Journal of Climate*, **32**(11),
505 3169-3187.
506 Hanna, E., Cropper, T. E., Hall, R. J., & Cappelen, J. (2016). Greenland Blocking Index 1851–2015:
507 a regional climate change signal. *International Journal of Climatology*, **36**(15), 4847-4861.
508 Hansen, A. R., & Sutera, A. (1993). A comparison between planetary-wave flow regimes and
509 blocking. *Tellus A: Dynamic Meteorology and Oceanography*, **45**(4), 281-288.
510 Hong, C. C., Hsu, H. H., Lin, N. H., & Chiu, H. (2011). Roles of European blocking and tropical-
511 extratropical interaction in the 2010 Pakistan flooding. *Geophysical Research Letters*, **38**(13).
512 Hsu, H. H. (1987). Propagation of low-level circulation features in the vicinity of mountain ranges.
513 *Monthly weather review*, **115**(9), 1864-1893
514 Hwang, J., Martineau, P., Son, S. W., Miyasaka, T., & Nakamura, H. (2020). The role of transient
515 Eddies in North Pacific blocking formation and its seasonality. *Journal of the Atmospheric*
516 *Sciences*, **77**(7), 2453-2470.

Jeong, D. I., Yu, B., & Cannon, A. J. (2021). Links between atmospheric blocking and North American winter cold spells in two generations of Canadian Earth System Model large ensembles. *Climate Dynamics*, 1-15.

Joung, C. H., & Hitchman, M. H. (1982). On the role of successive downstream development in East Asian polar air outbreaks. *Monthly Weather Review*, **110**(9), 1224-1237.

Jury, M. W., Herrera-García, S., Gutiérrez, J. M., Barriopedro, D. (2019). Blocking representation in the ERA-Interim driven EURO-CORDEX RCMs. *Climate Dynamics*, **52**(5), 3291–3306

Kim, K. Y., & Son, S. W. (2016). Physical characteristics of Eurasian winter temperature variability. *Environmental Research Letters*, **11**(4), 044009.

Kim, H. J., & Son, S. W. (2020). Eurasian winter temperature change in recent decades and its association with Arctic sea ice loss. *Polar Research*.

Kim, H. J., Son, S. W., Moon, W., Kug, J. S., & Hwang, J. (2021). Subseasonal relationship between Arctic and Eurasian surface air temperature. *Scientific reports*, **11**(1), 1-10.

Kim, S. H., & Kim, B. M. (2019). In search of winter blocking in the western North Pacific Ocean. *Geophysical Research Letters*, **46**(15), 9271-9280.

Kobayashi, S., Ota, Y., Harada, Y., Ebita, A., Moriya, M., Onoda, H., ... & Takahashi, K. (2015). The JRA-55 reanalysis: General specifications and basic characteristics. *Journal of the Meteorological Society of Japan. Ser. II*, **93**(1), 5-48.

Kushnir, Y. (1987). Retrograding wintertime low-frequency disturbances over the North Pacific Ocean. *Journal of Atmospheric Sciences*, **44**(19), 2727-2742.

Lau, W. K., & Kim, K. M. (2012). The 2010 Pakistan flood and Russian heat wave: Teleconnection of hydrometeorological extremes. *Journal of Hydrometeorology*, **13**(1), 392-403.

Luo, D., Xiao, Y., Yao, Y., Dai, A., Simmonds, I., & Franzke, C. L. (2016). Impact of Ural blocking on winter warm Arctic–cold Eurasian anomalies. Part I: Blocking-induced amplification. *Journal of Climate*, **29**(11), 3925-3947.

542 Lupo, A. R., & Smith, P. J. (1995). Climatological features of blocking anticyclones in the Northern
543 Hemisphere. *Tellus A*, **47**(4), 439-456.
544 MacDonald, G. M. (2007). Severe and sustained drought in southern California and the West:
545 Present conditions and insights from the past on causes and impacts. *Quaternary*
546 *International*, **173**, 87-100.
547 Maddison, J. W., Abalos, M., Barriopedro, D., García-Herrera, R., Garrido-Perez, J. M., & Ordóñez,
548 C. (2021). Linking air stagnation in Europe with the large-scale atmospheric circulation.
549 *Weather and Climate Dynamics Discussions*, 1-25.
550 Martineau, P., Chen, G., & Burrows, D. A. (2017). Wave events: Climatology, trends, and
551 relationship to Northern Hemisphere winter blocking and weather extremes. *Journal of*
552 *Climate*, **30**(15), 5675-5697.
553 Masato, G., Hoskins, B. J., & Woollings, T. J. (2012). Wave- breaking characteristics of midlatitude
554 blocking. *Quarterly Journal of the Royal Meteorological Society*, **138**(666), 1285-1296.
555 Masato, G., Woollings, T., & Hoskins, B. J. (2014). Structure and impact of atmospheric blocking
556 over the Euro- Atlantic region in present- day and future simulations. *Geophysical Research*
557 *Letters*, **41**(3), 1051-1058.
558 Matsueda, M. (2011). Predictability of Euro- Russian blocking in summer of 2010. *Geophysical*
559 *Research Letters*, **38**(6).
560 Miller, R. L., Lackmann, G. M., & Robinson, W. A. (2020). A New Variable-Threshold Persistent
561 Anomaly Index: Northern Hemisphere Anomalies in the ERA-Interim Reanalysis. *Monthly*
562 *Weather Review*, **148**(1), 43-62.
563 Mori, M., Watanabe, M., Shiogama, H., Inoue, J., & Kimoto, M. (2014). Robust Arctic sea-ice
564 influence on the frequent Eurasian cold winters in past decades. *Nature Geoscience*, **7**(12),
565 869-873.
566 Nakamura, N., & Huang, C. S. (2018). Atmospheric blocking as a traffic jam in the jet stream.

Science, **361**(6397), 42-47.

Ordóñez, C., Barriopedro, D., García-Herrera, R., Sousa, P. M., & Schnell, J. L. (2017). Regional responses of surface ozone in Europe to the location of high-latitude blocks and subtropical ridges. *Atmospheric Chemistry and Physics*, **17**(4), 3111-3131.

Park, T. W., Ho, C. H., & Yang, S. (2011). Relationship between the Arctic Oscillation and cold surges over East Asia. *Journal of Climate*, **24**(1), 68-83.

Park, T. W., Ho, C. H., & Deng, Y. (2014). A synoptic and dynamical characterization of wave-train and blocking cold surge over East Asia. *Climate dynamics*, **43**(3-4), 753-770.

Pfahl, S., & Wernli, H. (2012). Quantifying the relevance of atmospheric blocking for co-located temperature extremes in the Northern Hemispherere on (sub-) daily time scales. *Geophysical Research Letters*, **39**(12)

Scherrer, S. C., Croci- Maspoli, M., Schwierz, C., & Appenzeller, C. (2006). Two- dimensional indices of atmospheric blocking and their statistical relationship with winter climate patterns in the Euro- Atlantic region. *International Journal of Climatology: A Journal of the Royal Meteorological Society*, **26**(2), 233-249.

Shi, N., Tian, P., Wang, Y., & Wang, X. (2020). Contrasting Relationship between Wintertime Blocking Highs over Europe–Siberia and Temperature Anomalies in the Yangtze River Basin. *Monthly Weather Review*, **148**(7), 2953-2970.

Song, L., Wang, L., Chen, W., & Zhang, Y. (2016). Intraseasonal variation of the strength of the East Asian trough and its climatic impacts in boreal winter. *Journal of Climate*, **29**(7), 2557-2577.

Song, L., & Wu, R. Two types of Rossby wave breaking events and their influences on East Asian winter temperature. *Journal of Geophysical Research: Atmospheres*, e2020JD033917.

Sousa, P. M., Barriopedro, D., García-Herrera, R., Woollings, T., Trigo, R.M. (2021). A new combined detection algorithm for blocking and subtropical ridges. *Journal of Climate*, **34**(18), 7735-7758.

592 Sousa, P. M., Trigo, R. M., Barriopedro, D., Soares, P. M., Ramos, A. M., & Liberato, M. L. (2017).
593 Responses of European precipitation distributions and regimes to different blocking
594 locations. *Climate dynamics*, **48**(3), 1141-1160.
595 Sousa, P. M., Trigo, R. M., Barriopedro, D., Soares, P. M., & Santos, J. A. (2018). European
596 temperature responses to blocking and ridge regional patterns. *Climate Dynamics*, **50**(1), 457-
597 477.
598 Sung, M. K., Son, S. W., Yoo, C., Hwang, J., & An, S. I. (2021). Seesawing of winter temperature
599 extremes between East Asia and North America. *Journal of Climate*, **34**(11), 4423-4434.
600 Takaya, K., & Nakamura, H. (2005). Mechanisms of intraseasonal amplification of the cold Siberian
601 high. *Journal of the Atmospheric Sciences*, **62**(12), 4423-4440.
602 Takaya, K., & Nakamura, H. (2005). Geographical dependence of upper-level blocking formation
603 associated with intraseasonal amplification of the Siberian high. *Journal of the atmospheric*
604 *sciences*, **62**(12), 4441-4449.
605 Tibaldi, S., & Molteni, F. (1990). On the operational predictability of blocking. *Tellus A*, **42**(3), 343-
606 365.
607 Tibaldi, S., Tosi, E., Navarra, A., & Pedulli, L. (1994). Northern and Southern Hemisphere seasonal
608 variability of blocking frequency and predictability. *Monthly Weather Review*, **122**(9), 1971-
609 2003.
610 Tyrlis, E., & Hoskins, B. J. (2008). Aspects of a Northern Hemisphere atmospheric blocking
611 climatology. *Journal of the atmospheric sciences*, **65**(5), 1638-1652.
612 Tyrlis, E., Bader, J., Manzini, E., Ukita, J., Nakamura, H., & Matei, D. (2020). On the role of Ural
613 Blocking in driving the Warm Arctic–Cold Siberia pattern. *Quarterly Journal of the Royal*
614 *Meteorological Society*, **146**(730), 2138-2153.
615 Tyrlis, E., Bader, J., Manzini, E., & Matei, D. (2021). Reconciling different methods of high-
616 latitude blocking detection. *Quarterly Journal of the Royal Meteorological Society*, **147**(735),

1070-1096.

Wang, L., Chen, W., Zhou, W., Chan, J. C., Barriopedro, D., & Huang, R. (2010). Effect of the climate shift around mid 1970s on the relationship between wintertime Ural blocking circulation and East Asian climate. *International Journal of Climatology: A Journal of the Royal Meteorological Society*, **30**(1), 153-158.

Wiedenmann, J. M., Lupo, A. R., Mokhov, I. I., & Tikhonova, E. A. (2002). The climatology of blocking anticyclones for the Northern and Southern Hemispheres: Block intensity as a diagnostic. *Journal of Climate*, **15**(23), 3459-3473.

Woollings, T., Barriopedro, D., Methven, J., Son, S. W., Martius, O., Harvey, B., ... & Seneviratne, S. (2018). Blocking and its response to climate change. *Current Climate Change Reports*, **4**(3), 287-300.

Yao, Y., Luo, D., Dai, A., & Simmonds, I. (2017). Increased quasi stationarity and persistence of winter Ural blocking and Eurasian extreme cold events in response to Arctic warming. Part I: Insights from observational analyses. *Journal of Climate*, **30**(10), 3549-3568.

Yihui, D. (1990). Build-up, air mass transformation and propagation of Siberian high and its relations to cold surge in East Asia. *Meteorology and Atmospheric Physics*, **44**(1), 281-292

Yoo, Y. E., Son, S. W., Lee, J. H., & Min, S. K. (2019). Abrupt Decrease of Wintertime Cold Nights in Korea in the Late 1980s. *Asia-Pacific Journal of Atmospheric Sciences*, **55**(1), 31-39.

Yun, S. G., & Yoo, C. (2019). The Effects of Spring and Winter Blocking on PM10 Concentration in Korea. *Atmosphere*, **10**(7), 410.

Table 1. The number of UR and OK blocking events detected by three blocking indices during the extended winters of 1979-2018. Common cases are defined when one index detects blocking onset, and the other two indices also detect blocking within two days of the blocking onset.

	ANO	MIX	REV	Common
Ural	118	90	109	59
Okhotsk	86	66	89	39

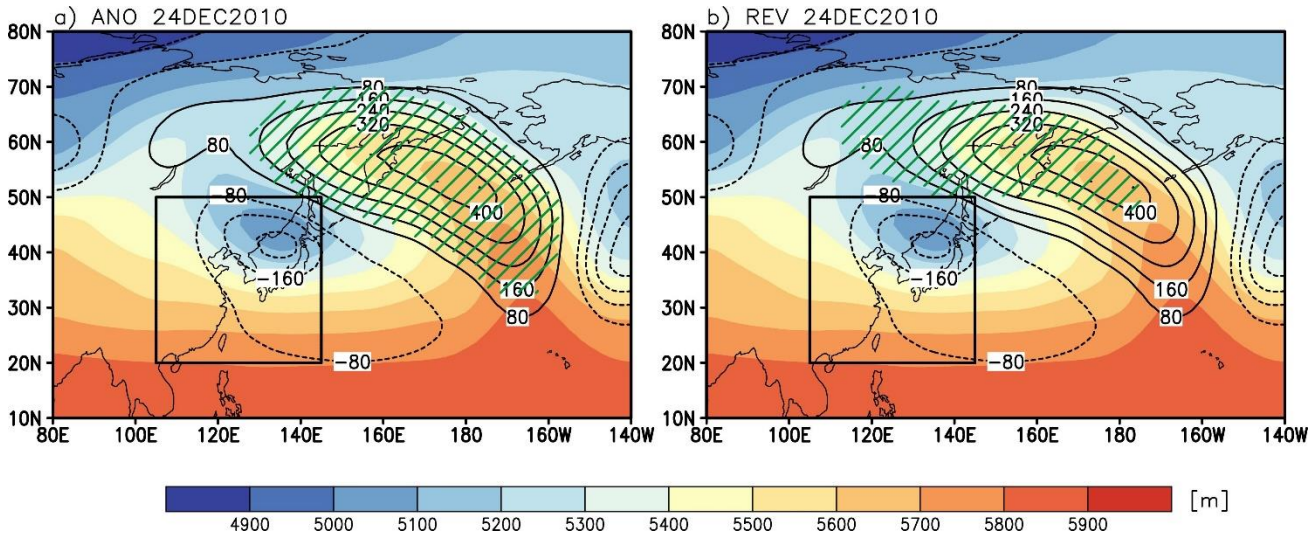

641

642 **Figure 1.** Z500 (shading, in m) and Z500 anomaly (contours) on 24 December 2010. The hatched area shows

643 the region where blocking is detected by the (a) ANO and (b) REV indices. The black box indicates the East

644 Asian domain (105ºE-145ºE, 20ºN-50ºN). The contour interval is 20 m. Zero line is omitted.

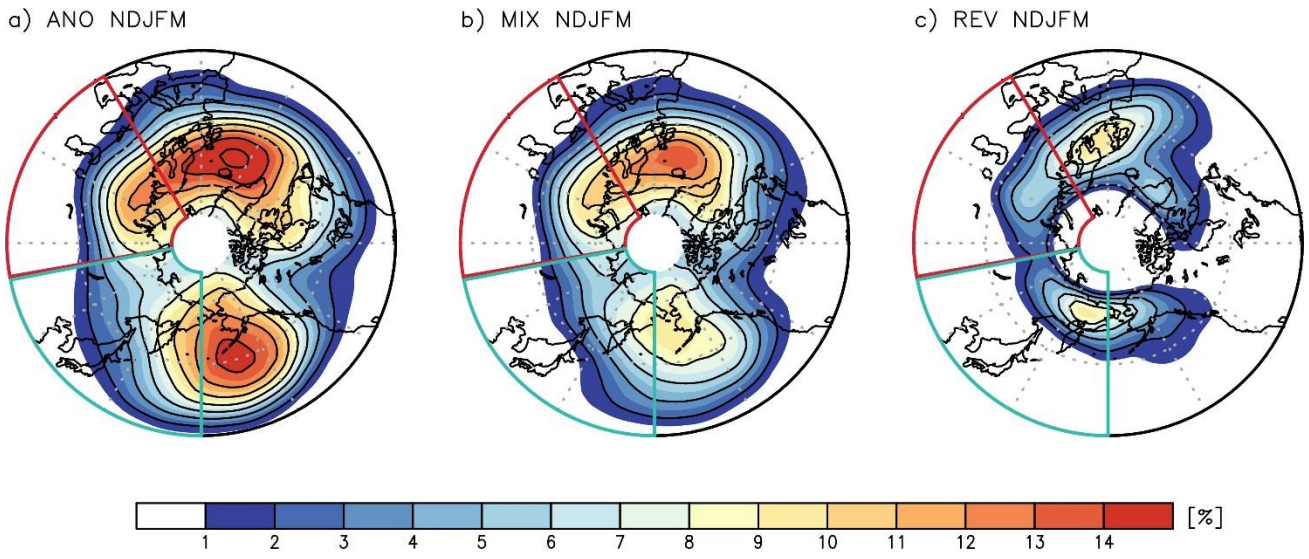

645

646 **Figure 2.** Climatology (1979-2018) of winter blocking frequency (in percentage of days of the extended winter
647 season) detected by each blocking index: a) ANO, b) MIX, and c) REV. Contour interval is 2%. Red and green
648 boxes indicate the Ural (30º-100ºE) and Okhotsk (100º-180ºE) regions, respectively.

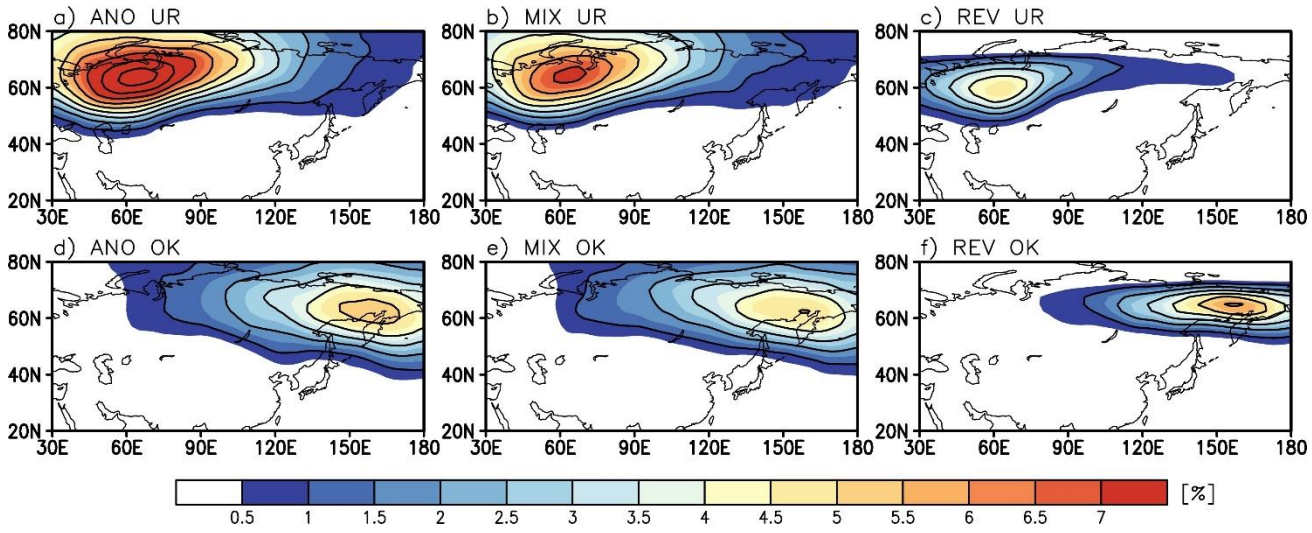

649

650 **Figure 3.** Same as Fig. 2 but only for (top) Ural and (bottom) Okhotsk blocking events. Note that shading and

651 contour intervals are halved as compared to Fig. 2.

652

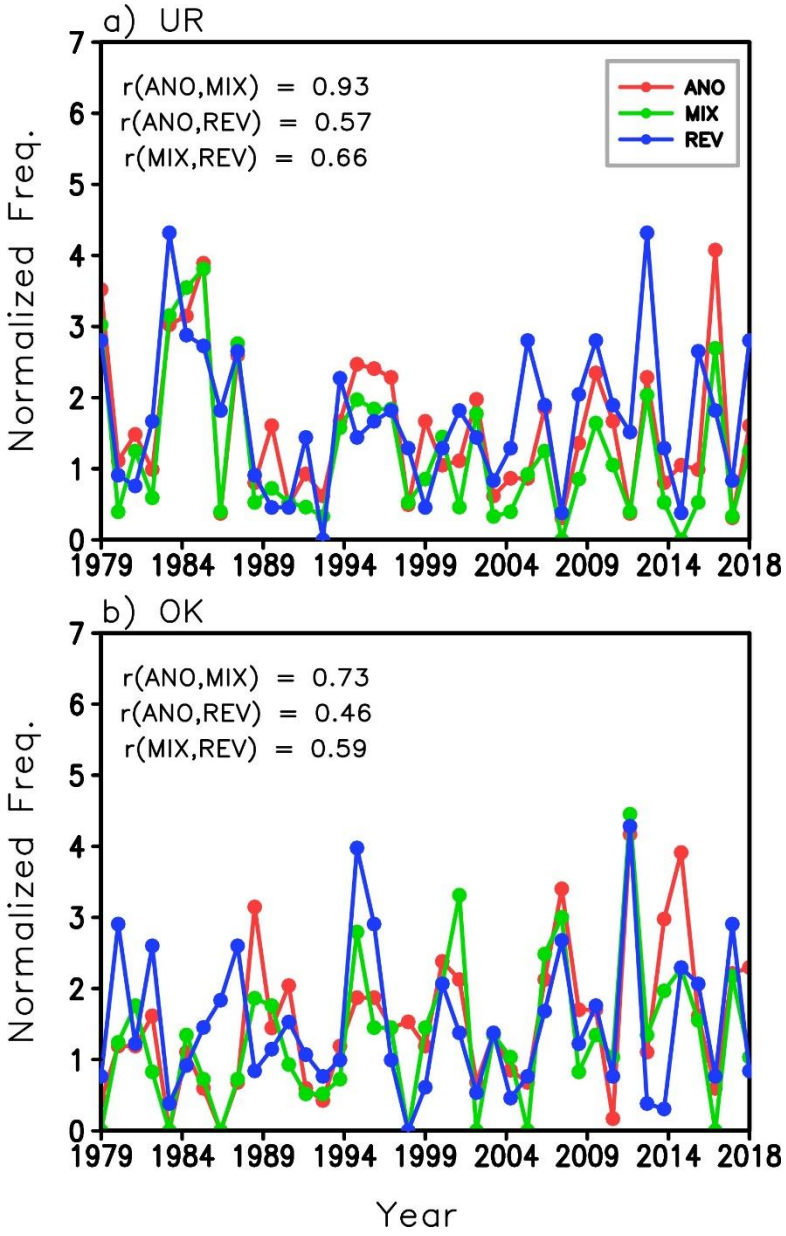

Figure 4. Time series of (a) UR and (b) OK blocking frequencies during the extended winter. Red, green, and blue lines denote the normalized blocking frequencies detected by the ANO, MIX, and REV indices, respectively. Correlation coefficients between the time series of blocking index frequencies are also shown.

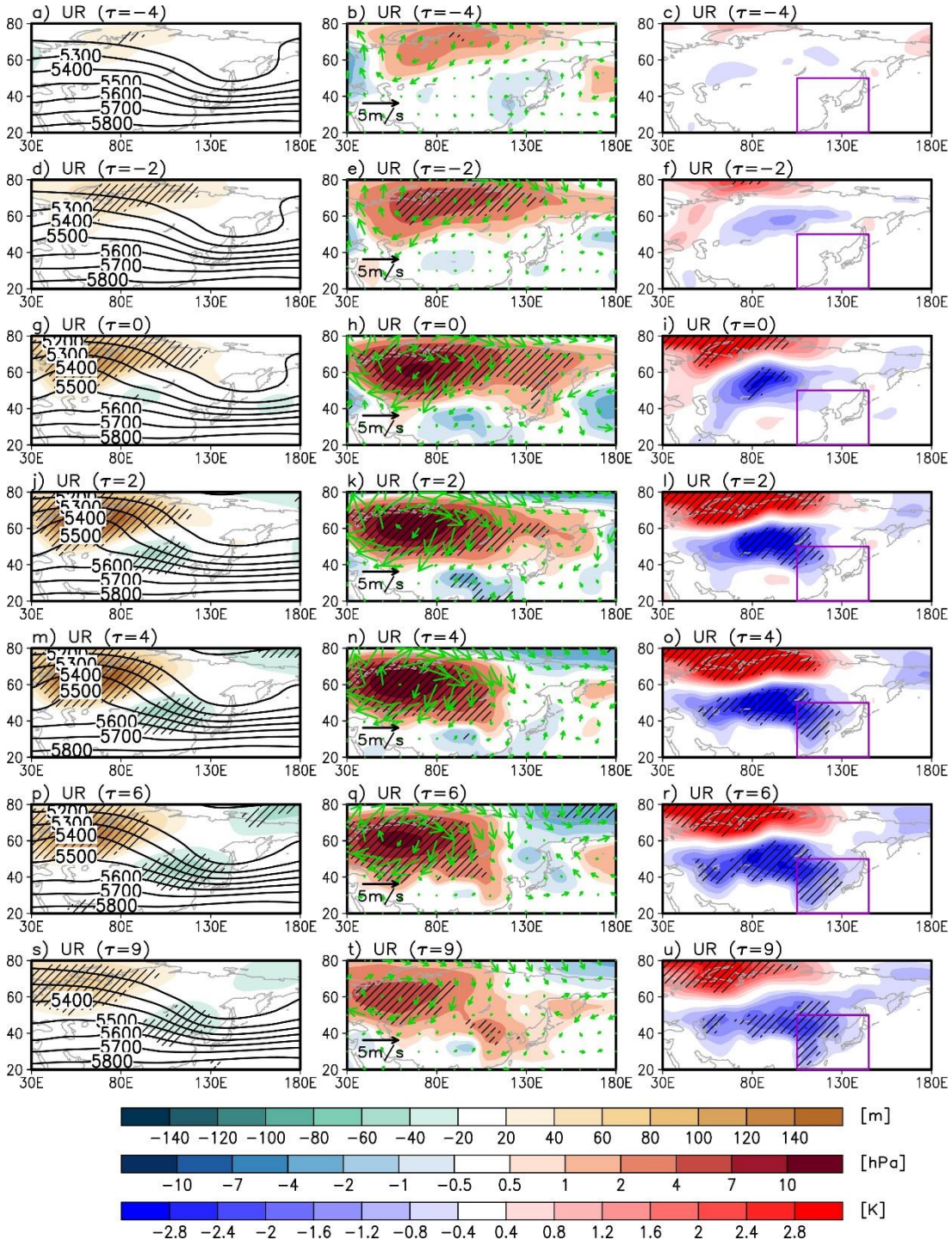

Figure 5. Spatio-temporal evolution of (left) Z500 (contour, in m) and its anomaly (shading), (middle) MSLP anomaly (shading, in hPa), and horizontal wind vector anomaly at 925 hPa (vectors, in m s^{-1}), and (right) SAT anomaly (shading, in K) from lag -4 to 9 days with respect to Ural blocking onset. Contour interval of Z500 is 100 m. The values which are statistically significant at the 95% confidence level (two-tailed t-test) in all three blocking indices are hatched. The purple box indicates the East Asian domain (105º-145ºE, 20º-50ºN).

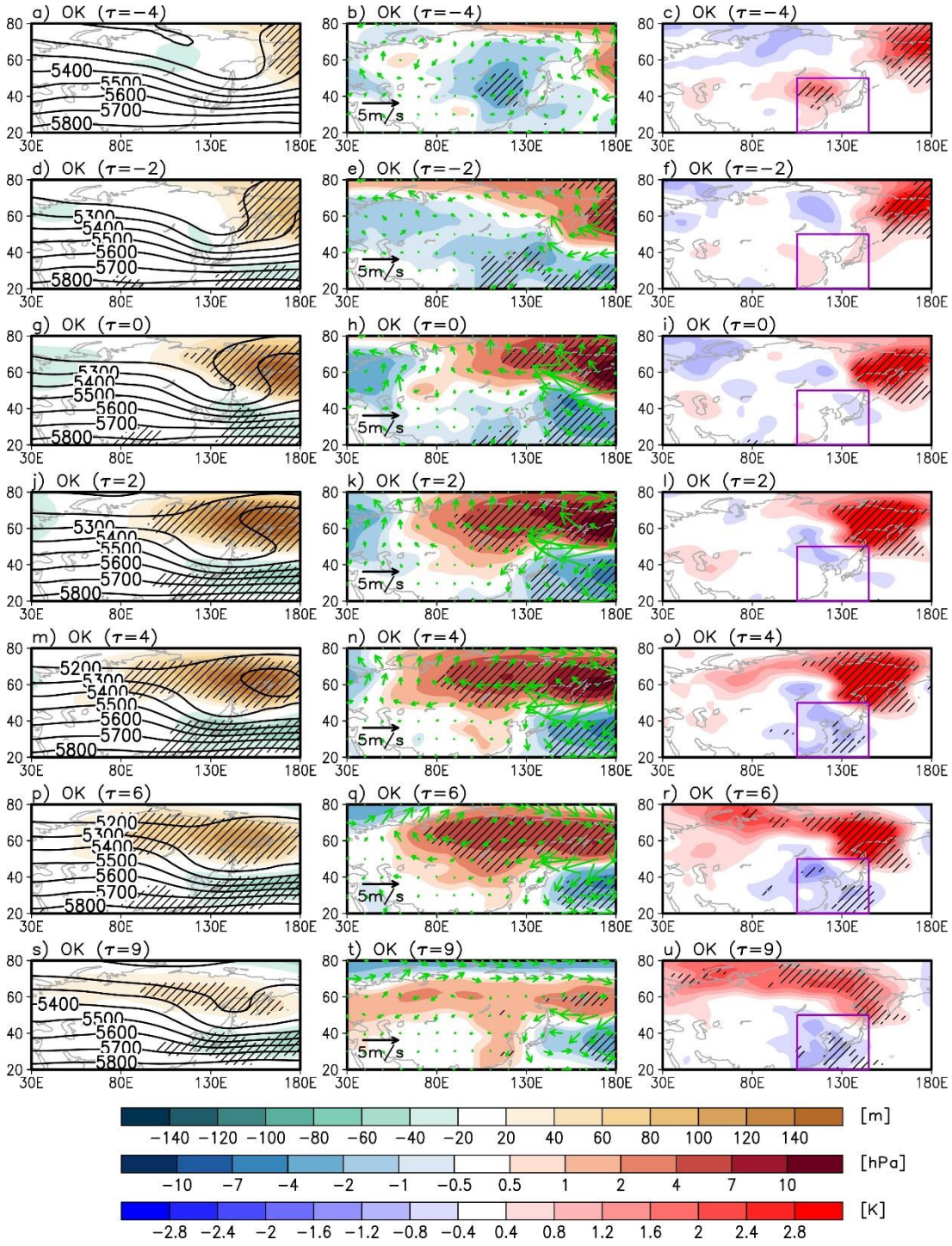

Figure 6. Same as Fig. 5 but for Okhotsk blocking.

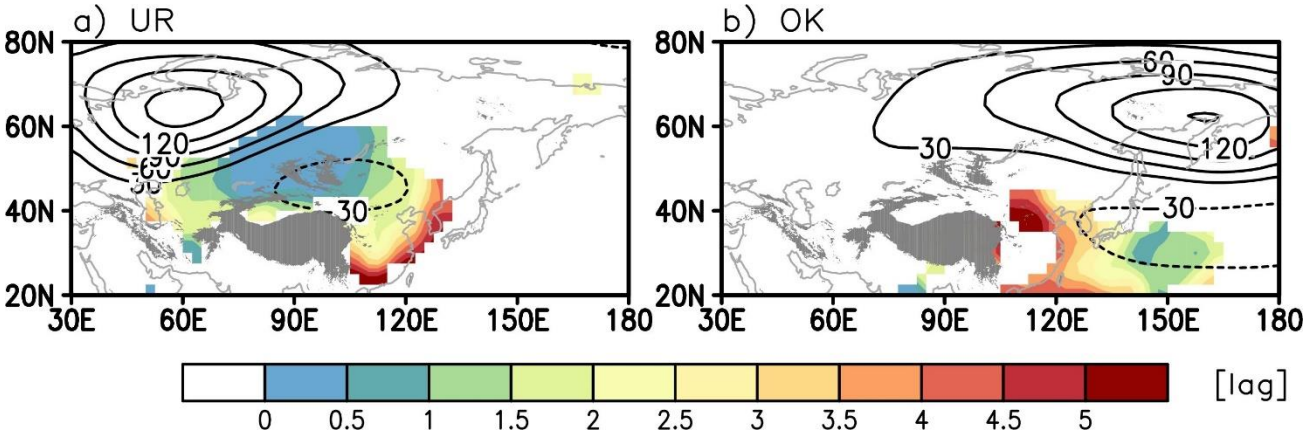

666

667 **Figure 7.** The response time of SAT to (a) Ural and (b) Okhotsk blocking events. The response time is defined
668 as the first day when the negative SAT anomaly becomes statistically significant at the 95% confidence level.
669 Unit is day. Only the values which are statistically significant in all three indices are shaded. The composite of
670 Z500 anomaly at the blocking onset day is contoured. Zero line is omitted. The gray shading denotes the regions
671 with a surface elevation higher than 2000 m.

672

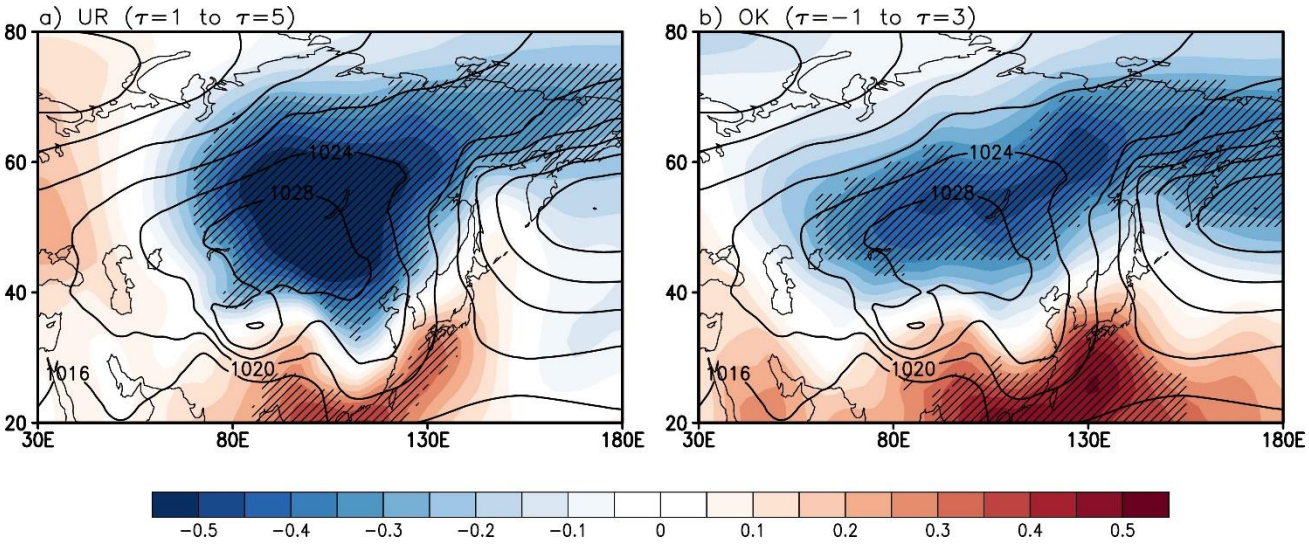

673

674 **Figure 8.** Correlation map (shading) between MSLP anomaly and East Asian SAT tendency for (a) Ural and (b)
675 Okhotsk blocking events. Contours denote the climatology of MSLP for the extended winter. Hatching indicates
676 statistically significant values at the 95% confidence level for the three blocking indices. Contour interval is 4
677 hPa.

678

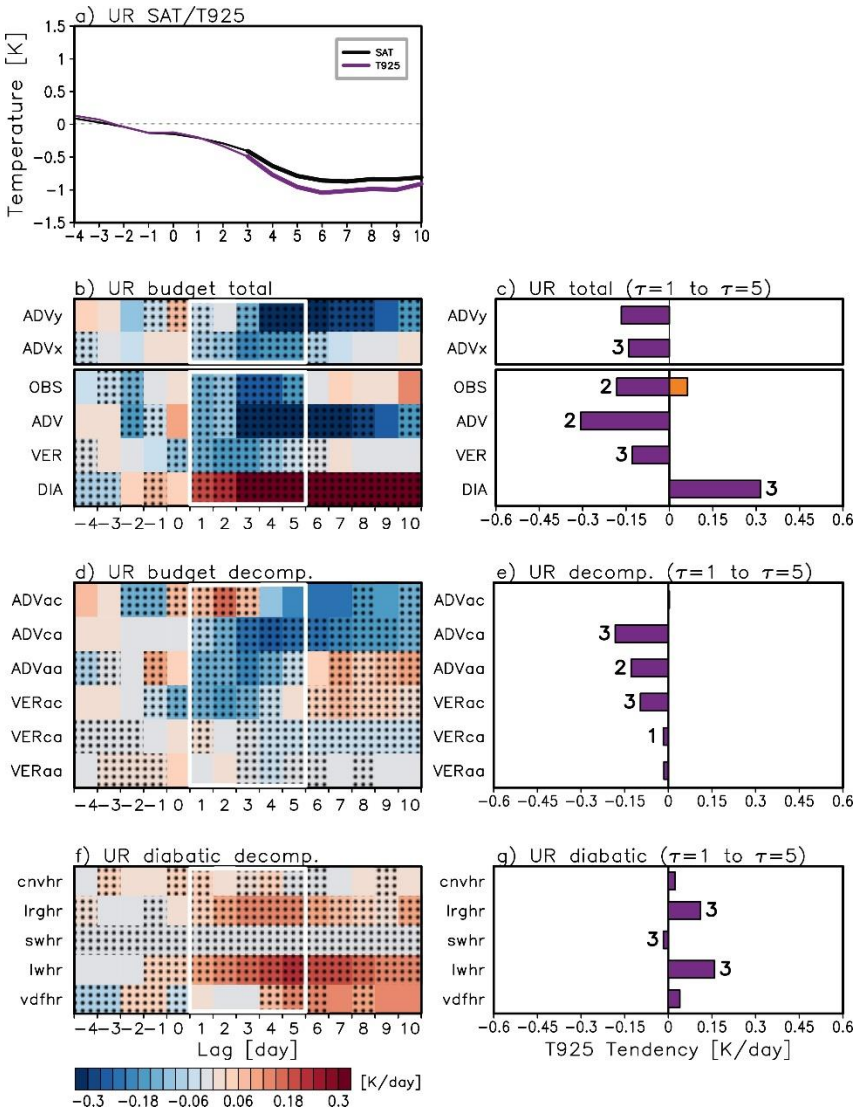

679

680 **Figure 9.** Time evolution of (a) East Asian SAT and T925 anomalies (in K), (b) T925 tendency budget (Eq. (3)
681 in K day-1), the decomposed components of (d) horizontal advection and adiabatic heating terms (in K day-1;
682 see Eqs. (4) and (5) for details), and (f) the individual components of the terms (in K day-1; see Eq. (3)), from
683 lag -4 to 10 days with respect to Ural blocking onset. Bold lines in (a) denote statistically significant values at
684 the 95% confidence level in all three blocking indices. The values showing the same sign in all three blocking
685 indices are dotted in (b), (d), and (f). (c) Contributing terms to T925 tendency averaged from lag 1 to 5 days
686 (white box in (b)). Residual of the budget tendency is denoted with an orange bar. (e, g) As (c) but for the
687 decomposed terms. The number of blocking indices with statistically significant values at the 95% confidence
688 level is indicated in (c), (e), and (g).

689

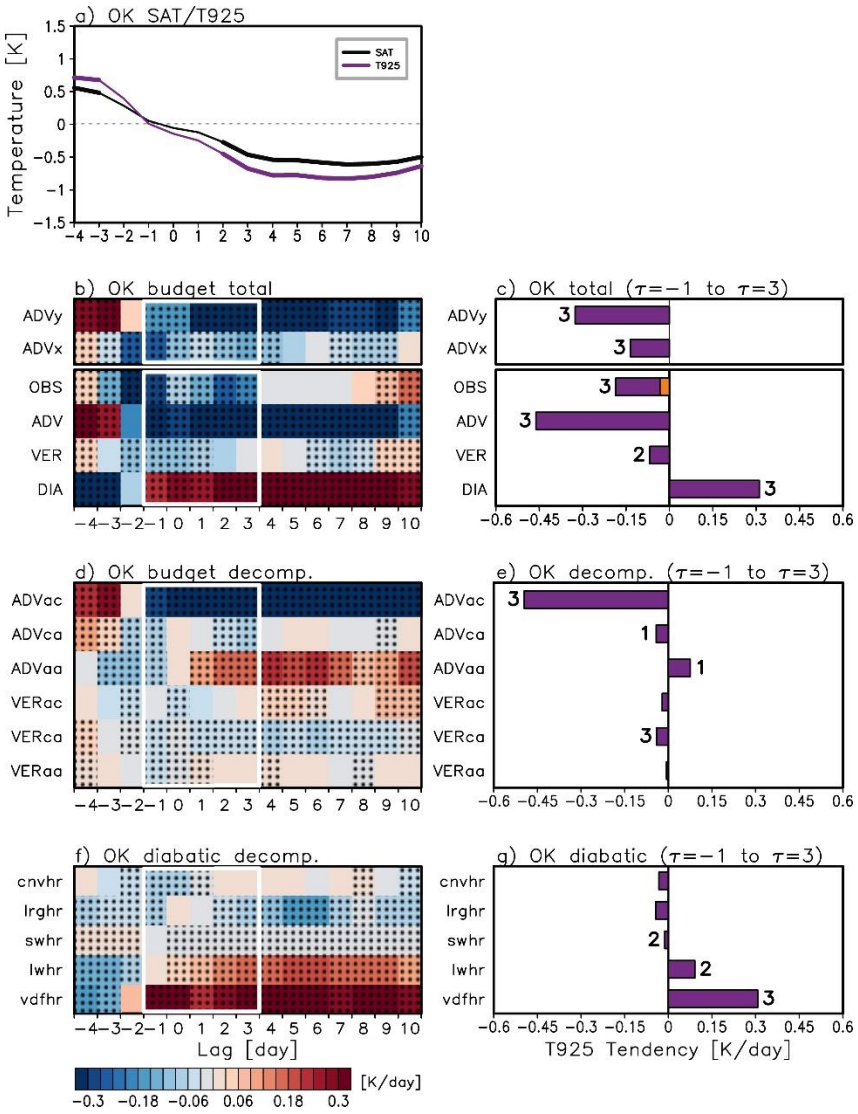

690

691 **Figure 10.** Same as Fig. 9 but for Okhotsk blocking.

Supporting information for:

Impact of winter blocking on surface air temperature in East Asia: Ural versus Okhotsk blockings

Jaeyoung Hwang[1], Seok-Woo Son[1]

Patrick Martineau[2], and David Barriopedro[3]

1. School of Earth and Environmental Sciences, Seoul National University, Seoul, Republic of Korea.
2. Japan Agency for Marine-Earth Science and Technology, Yokohama, Japan
3. Instituto de Geociencias, Consejo Superior de Investigaciones Científicas - Universidad Complutense de Madrid (CSIC-UCM), Madrid, Spain

Corresponding Author: Seok-Woo Son, School of Earth and Environmental Sciences, Seoul National University, 1 Gwanak-ro, Gwanak-gu, Seoul 08826, Republic of Korea.

E-mail: seokwooson@snu.ac.kr. Phone: +82-2-880-8152.

716

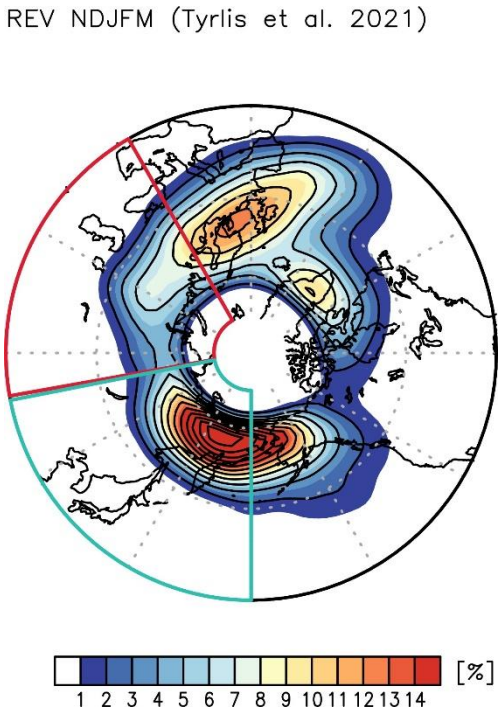

717

718 **Figure S1.** Same as Fig. 2c but for REV index with a lessened poleward criterion as in Tyrlis et al. (2021).

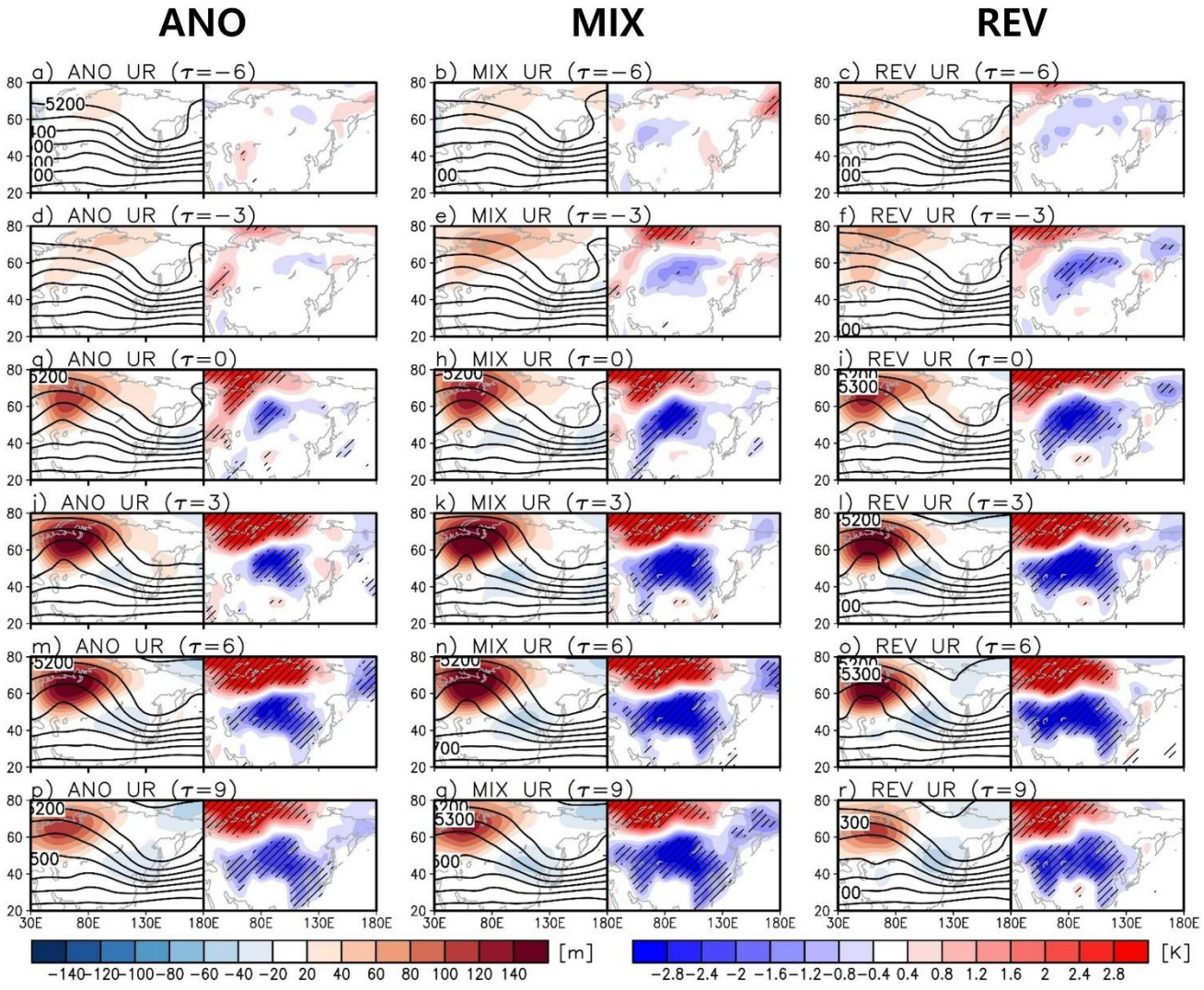

Figure S2. Time evolution of Z500 (left contour, in m), its anomaly (left shading), and SAT anomaly (right shading, in K) from lag -6 to 9 days with respect to Ural blocking onset. Hatching denotes statistically significant SAT anomalies with respect to climatology at the 95% confidence level (two-tailed t-test). From left to right, retults for the ANO, MIX, and REV indices are shown as in Fig. 5.

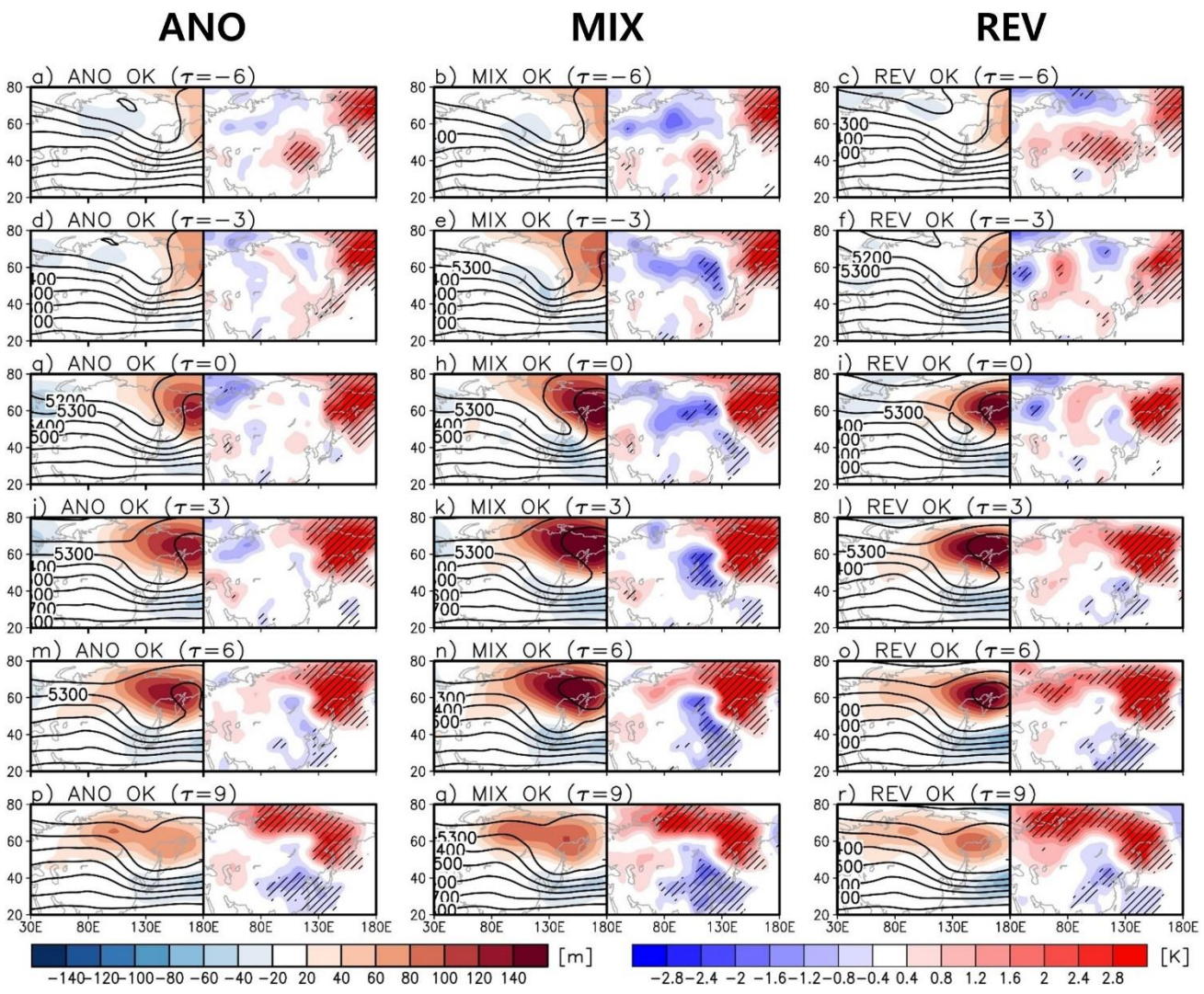

Figure S3. Same as Fig. S2 but for Okhotsk blocking.

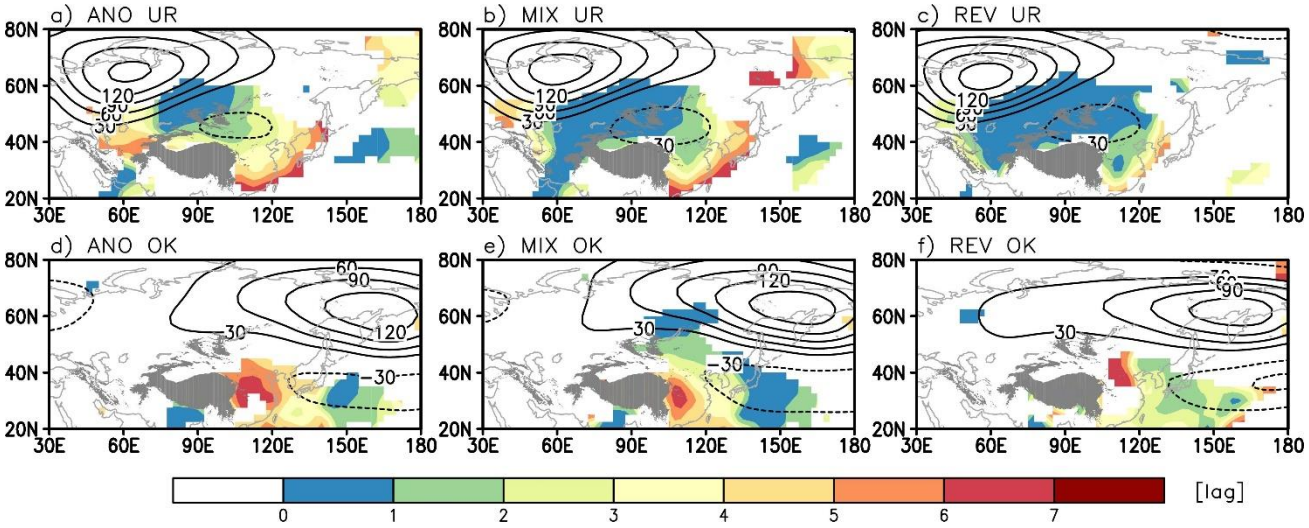

738

739 **Figure S4.** The response time of SAT to (top) Ural and (bottom) Okhotsk blocking events detected by ANO
740 (left), MIX (middle), and REV (right) indices. Unit is day. Contours show the composited Z500 anomaly at the
741 onset day, with 30 m intervals. Zero line is omitted. The gray shading denotes the regions with a surface
742 elevation higher than 2000 m.

743

744

745

746

747

748

749

750

751

752

753

754

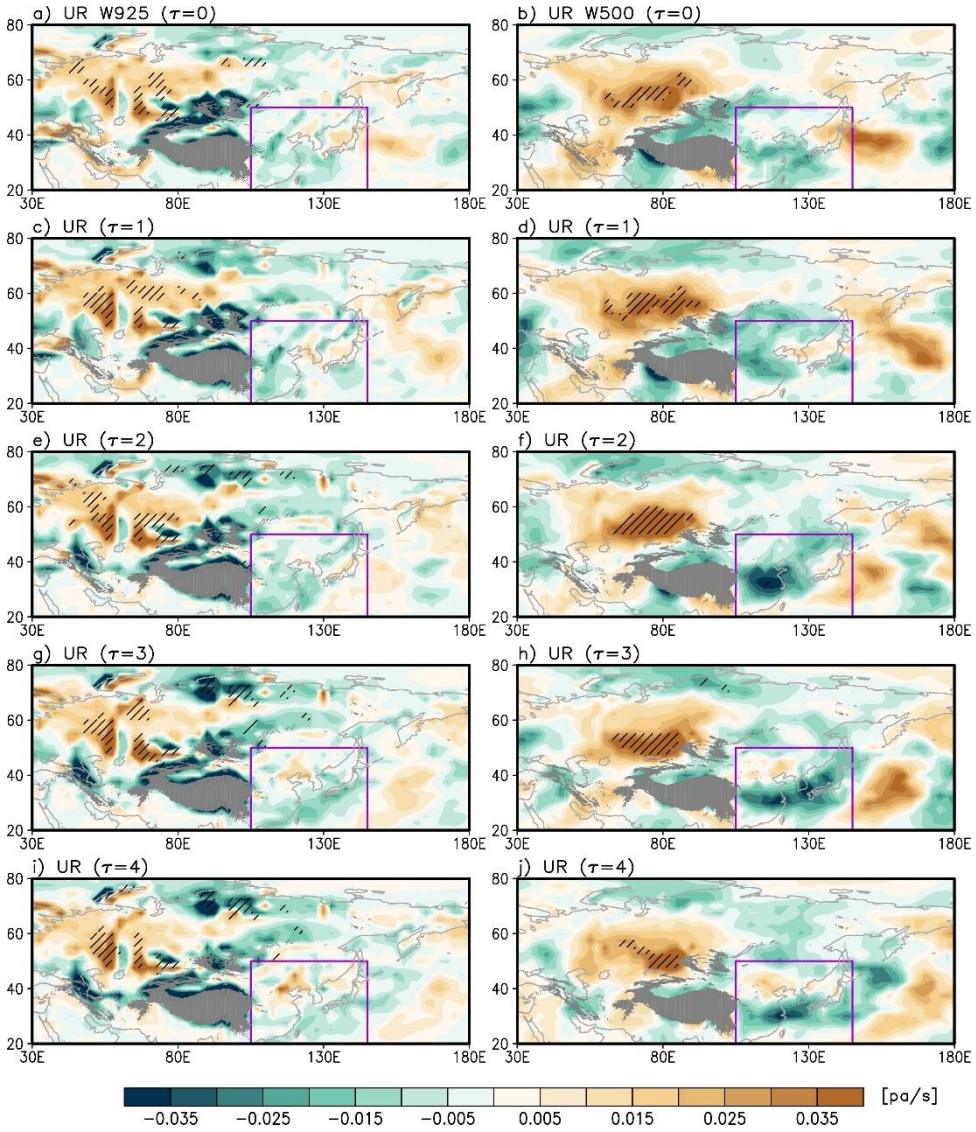

755

756 **Figure S5.** Composite of vertical velocity (Pa s^{-1}) at (left) 925 hPa and (right) 500 hPa from lag 0 to 4 days with
757 respect to Ural blocking onset. Statistically significant values at the 95% confidence level (two-tailed t-test) and
758 with the same signed anomaly in all three blocking indices are hatched. The purple box indicates the East Asian
759 domain (105º-145ºE, 20º-50ºN). Gray shading denotes the regions with a surface elevation higher than 2000 m.